# Reconstruction of Sparsely Sampled Seismic Data via Residual U-Net

Shuhang Tang, Yinshuai Ding<sup>®</sup>, Hua-Wei Zhou, and Heng Zhou

Abstract—Reconstruction of sparsely sampled seismic data is critical for maintaining the quality of seismic images when significant numbers of shots and receivers are missing. We present a reconstruction method in the shot-receiver-time (SRT) domain based on a residual U-Net machine learning architecture, for seismic data acquired in a sparse 2-D acquisition and name it SRT2D-ResU-Net. The SRT domain retains a high level of seismic signal connectivity, which is likely the main data feature that the reconstructing algorithms rely on. We develop an "in situ training and prediction" workflow by dividing the acquisition area into two nonoverlapping subareas: a training subarea for establishing the network model using regularly sampled data and a testing subarea for reconstructing the sparsely sampled data using the trained model. To establish a reference base for analyzing the changes in data features over the study area, and quantifying the reconstructed seismic data, we devise a baseline reference using a tiny portion of the field data. The baselines are properly spaced and excluded from the training and reconstruction processes. The results on a field marine data set show that the SRT2D-ResU-Net can effectively learn the features of seismic data in the training process, and the average correlation between the reconstructed missing traces and the true answers is over 85%.

Index Terms—Baseline reference, convolutional neural network, deep residual U-Net, reconstruction.

# I. INTRODUCTION

THE quality of seismic images of the earth's structures relies on regularly and densely sampled seismic data in field acquisitions, which provide angular illumination of the subsurface targets with sufficiently high signal-to-noise ratio (SNR) [1], [2]. However, sparsely sampled data sets do occur in field practice due to various reasons, chiefly the existence of survey obstacles and the limitations in the financial and time budgets of seismic surveys. While maintaining high image quality is a key in designing and processing of seismic data, the cost of seismic surveys increases greatly with the increasing numbers of shots and receivers. Interestingly, recent developments of sparse sampling (compressive sensing) in signal processing offer a way to save the acquisition cost and maintain the image quality at the same time [3], [4]. The desired data sparsity in space is realized by intentionally reducing the shots and receivers to smaller numbers; after

Manuscript received May 30, 2020; revised July 20, 2020 and August 25, 2020; accepted October 26, 2020. This work was supported in part by the NSF under Grant OCE-1832197. (Corresponding author: Yinshuai Ding.)

Shuhang Tang and Hua-Wei Zhou are with the Department of Earth and Atmospheric Sciences, University of Houston, Houston, TX 77004 USA.

Yinshuai Ding is with the Department of Earth and Atmospheric Sciences, University of Houston, Houston, TX 77004 USA, and also with the Department of Earth Sciences, Uppsala University, 75236 Uppsala, Sweden (e-mail: yinshuai.ding@geo.uu.se).

Heng Zhou is with BGP International, BGP Inc., Zhuozhou 072751, China. Color versions of one or more of the figures in this letter are available online at https://ieeexplore.ieee.org.

Digital Object Identifier 10.1109/LGRS.2020.3035835

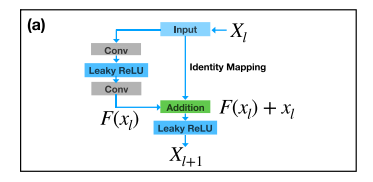
field acquisition, regularly sampled data can be reconstructed in computer from the sparsely sampled seismic data [5], [6]. The quality of the reconstructed data depends mostly on the sparsity of the data and, to a lesser but still significant extent, the reconstruction method.

In this letter, we exploit the potential of using machine learning (ML) in the reconstruction of sparsely sampled seismic data, particularly reflection seismic profiles acquired in exploration geophysics. ML has achieved success in many areas, such as medical imaging and remote sensing, as well as in the reconstruction of seismic data using ML networks [7]–[11]. Interpolation of seismic data in the 2-D shot-gather domain, for example, was done by Jia and Ma [7] using support vector machine, by Mandelli *et al.* [8] using U-Net, and by Wang *et al.* [9] using Res-Net. Dictionary learning [10] and tight frame learning [11] were also applied to reconstruct seismic data. However, it is challenging for a single network to characterize seismic data universally [9], because the accuracy of the network decreases with the increasing difference in data features between the training area and the testing area.

To cope with the above challenge, we propose to reconstruct the sparsely sampled seismic data in the shot-receiver-time (SRT) domain using residual U-Net and name the algorithm SRT2D-ResU-Net. U-Net is a convolutional neural network that has already showed success in medical imaging when limited images are available [12], and in seismic applications [13]. As we use a U-Net with deep layers, we have added residual unit [14]–[16] in U-Net to ease the training of deep networks. The residual unit was first proposed by He et al. [14], by adding a skip-path to the addition unit, to facilitate an improved learning of deep layers. Zhang et al. [15] used ResU-Net in road extraction. To realize the in situ training and prediction in our SRT2D-ResU-Net, we have developed an "in situ training and prediction" workflow, by dividing the acquisition area into two nonoverlapping subareas. In the training subarea, the network is trained using regularly sampled data. In the testing or predicting subarea, the trained network is applied to reconstruct the sparsely acquired data. Typically, the size of the testing subarea is much larger than that of the training subarea.

In the SRT domain, S stands for the shot location, R stands for the receiver location, and T stands for the two-way travel time of seismic reflections. Hence, for 2-D seismic acquisition, a slice of the 3-D SRT data cube at a fixed shot location is a common shot slice, and a slice of the data cube at a fixed receiver location is a common receiver slice when receivers are not moving. We prefer to use the SRT domain for reconstructing sparsely sampled seismic data, since the connectivity of seismic signals is among the most important

1545-598X © 2020 IEEE. Personal use is permitted, but republication/redistribution requires IEEE permission. See https://www.ieee.org/publications/rights/index.html for more information.



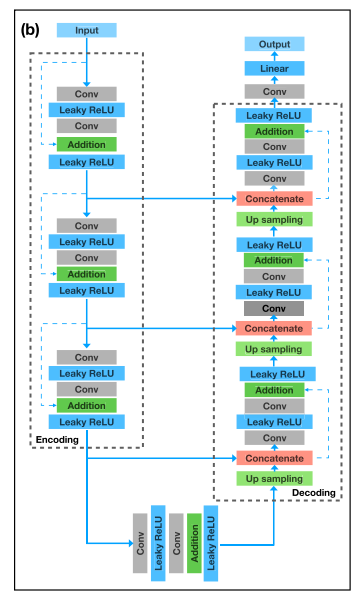


Fig. 1. Architectures of ResU-Net. (a) Residual block in U-Net. (b) Architecture of the designed ResU-Net. The blue arrowed lines indicate the skipping paths. The dashed blue arrowed lines indicate the identity mappings.

data features that the ML algorithms rely on. The SRT domain retains a high level of signal connectivity for continuous features such as seismic wavefields, as well as for piecewise continuous features with truncations, such as reflections from faulted rock strata.

It is infeasible to quantify the performance of the trained network for field data, because there are no measured values for their missing traces. To evaluate the performance of the trained network across the data cube, we devise a baseline reference as a quality control (QC) measure of the network. The baseline reference consists of a small number of field data traces, as the ground truth of the observed values distributed regularly over the entire survey area. All baseline traces, or baselines, are excluded from the training and treated as missing traces in the reconstructing processes. Since baselines have a similar distribution as the other missing traces, the performance of the network at the baselines can be used as a reliable indicator about the quality of the reconstructed traces. The baseline reference also enables an assessment about the changing data features from the training subarea to the testing subarea, as to be illustrated with a field marine data set in the following.

## II. METHODOLOGY

We choose the ResU-Net to accomplish the reconstruction. The ResU-net architecture includes an encoding path and a decoding path (Fig. 1). The skip-connections, which connect the encoding and decoding paths, help the network to combine data features from different levels. In the encoding path, we repeatedly apply the residual block [Fig. 1(a)]. Each residual block contains two convolution layers with kernel size

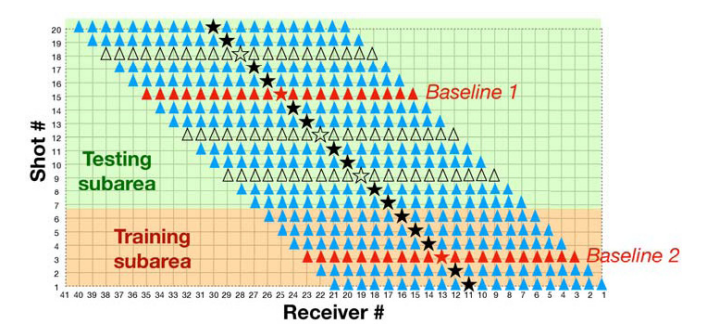


Fig. 2. Sketch of the shot/receiver coordinate system in a 2-D acquisition plan. The stars are shots and the triangles are receivers; there are 20 receivers per shot. The training subarea (yellow area with shots 1–6) has a regular sampling on the full grids. The testing subarea (green area with shots 7–20) has a sparse sampling, with blank triangles and stars indicating missing receivers and shots, respectively. Two baselines are indicated by the red stars and triangles.

 $3 \times 3 \times 3$ , two leaky rectified linear units (Leaky ReLU) [17], and one identity mapping. The down sampling between two residual blocks is realized by the first convolution layer with stride 2 in the second residual block. In the first level, we use 32 feature channels for the convolution, and the number of feature channels is doubled in each successive residual block. In the decoding path, we use a  $2 \times 2 \times 2$  "up sampling" layer, which doubles the inputs via repetition in each dimension, respectively, and then followed by a residual block. The data from the encoding path are passed by the skipping connections and then concatenated to the data from the corresponding layers in the decoding path [Fig. 1(b)]. The final layer is a  $1 \times 1 \times 1$  convolution layer with linear activations, which resizes the outputs as the size of inputs. We implement our ResU-Net architecture with Keras in Tensorflow [18], [19].

In the training stage, we use the data acquired on the full regular grids in the training subarea (Fig. 2) as the desired output in our supervised algorithm. To fulfill the goal of reconstruction using ResU-Net, we need the sparsely sampled data corresponding to the labeled data as inputs. Such sparsely sampled data could be acquired by reducing the shots and receivers, either randomly or regularly. For the 2-D seismic data, both the full data and the sparsely sampled data are in the 3-D SRT domain. To get the patch data which are suitable for training the ResU-Net, we extract a large number of 3-D boxed-data (size of  $32 \times 32 \times 32$ ) in the 3-D full data and the sparsely sampled data.

In the testing stage, we apply the trained model to the sparsely sampled data in the testing subarea (Fig. 2) and reconstruct the missing data there. In our field data test as an example, the sparsely sampled data are created by omitting every third shot from the testing subarea. Together with the baseline data, we have a missing rate around 30%.

In field studies, true values are unavailable for missing traces. The baselines should be chosen at the stage of acquisition design, as a tiny portion of the field data taking away from the training and reconstruction processes. Although the baseline traces are chosen artificially, they are preferably regularly spaces, as the ground truth for quantifying how well the network has been performed in the training and reconstruction stages. In our testing case in Section III, for

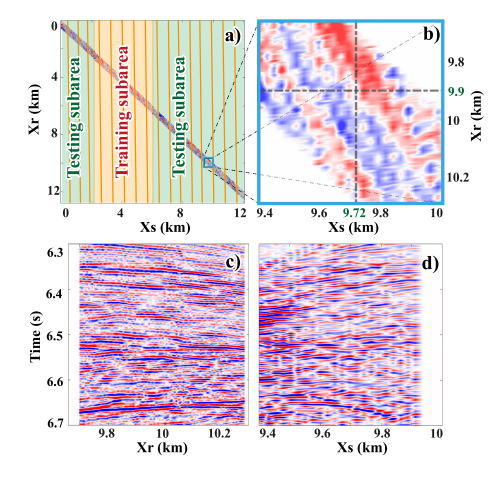


Fig. 3. Four slices of the SRT data cube. (a) Full data on a saturable reactor (SR) slice, showing two subareas and a small blue box locating the other slices. The orange vertical lines denote the baselines. (b) Zoomed-in time slice (t = 6.5 s) of the boxed area in (a); two dash lines are intersecting lines with slices (c) and (d). (c) Common shot slice (X = 9.72 km). (d) Common receiver slice (X = 9.9 km).

example, we take every 30th shot of the whole data set as the baseline shots, so the baselines count for 3.3% of the data set.

In the training stage, by removing the baseline shots from the data cube in the training sub area, we create gaps with not a number (NaN) values at baseline locations. Then, we need to condense the rest of the data cube as if there is no gap, to facilitate a proper network training using the condensed data cube. In the testing stage, we treat the baselines the same way as that for the missing traces. Based on the known true values of the baselines, their correlations with the reconstructed traces in the training subarea indicate how well we have trained the model; similarly, the correlations in the testing subarea indicate the performance of the trained model in the reconstruction.

## III. FIELD DATA SET EXPERIMENT

To evaluate the performance of the SRT2D-ResU-Net method, we tested it with several synthetic and field data sets. Here, we show the results for a field marine data set which was acquired in November 2019 in the South Atlantic Ocean. The purpose of the survey is to map ocean floor sediments, to assist the selection of future drilling sites. One of the 2-D seismic lines from the survey is selected for our experiment. This 2-D line has 503 shots, and each shot has 96 receivers (channels). The shot interval and the receiver interval are 24 and 6.25 m, respectively. The time sample interval is 1 ms, and the recording length is 8 s. The main frequency of the reflection data is around 120 Hz. Since the primary reflections from the targeted ocean floor sediments are between 6.3 and 6.7 s in the two-way travel time, after a preliminary processing, we use the data between 6.3 and 6.7 s to test our reconstruction method.

We transfer the data into a 3-D cube in the SRT domain (Fig. 3). The 3-D mesh grid of the SRT data cube is  $503 \times 2135 \times 401$ . From the whole data set of 503 shot gathers, we select 150 shot gathers (from shot 101 to 250) as the training subarea, including 100 (101–200) shot gathers as the training data and 50 (201–250) shot gathers as the validation data. The rest of the data set forms the testing subarea.

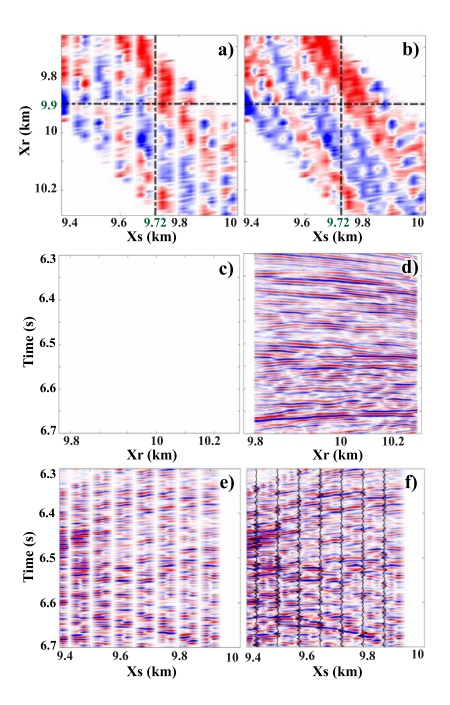


Fig. 4. Six slices of the SRT data cube illustrating the reconstruction of missing traces, in the same zoomed-in area as Fig. 3(b). (a) Time slice (t = 6.5 s) showing gaps due to missing eight shots. (b) Same time slice as (a), after reconstruction. Two black dash lines are the intersecting lines of these perpendicular slices. (c) and (d) Common shot slices at Xs = 9.72 km, before and after reconstruction. (e) and (f) Common receiver slices at Xr = 9.9 km before and after reconstruction. The black wiggle traces in (f) highlight seven reconstructed traces on this slice.

Thus, the sizes of the training subarea and testing subarea are about 30% and 70% of the whole data cube, respectively.

Fig. 3(a) shows a time slice at 6.5 s of the SRT data cube for the field 2-D survey. It is a plot of recorded data amplitude as a function of the shot location Xs and receiver location Xr. Fig. 3(b) shows the zoomed-in view of a small boxed area in Fig. 3(a), showing two intersecting lines of three perpendicular slices [Fig. 3(b)–(d)]. Fig. 3(c) shows a common shot slice, same as the common shot gather, a collection of seismic records of one shot by the streamer. Fig. 3(d) shows a common receiver slice, a collection of seismic records from many shots fired at different times to a fixed recording location. Since the hydrophone streamer sails following the air gun shots during the survey, a common receiver slice like Fig. 3(d) differs from a common receiver gather. Such common receiver slices are noisier than common shot slices (common shot gathers).

We train the ResU-Net model with 100 epochs. The loss function (in terms of L2 norm) in the network is defined as  $L(w) = ||\text{Net}(D_1, w) - D_0||_2^2$ , where w denotes the network parameters. With the convergence of the loss function, we obtain the trained model, which is used in reconstructing all the missing traces in the data cube.

### IV. ANALYSIS OF EXPERIMENTAL RESULTS

Fig. 4 illustrates the reconstruction result in comparison to the field data on three intersecting slices, in the same zoomed-in box in Fig. 3(a). The top pair of the panels [Fig. 4(a) and (b)] compares the time slices, the middle pair

TABLE I

MEAN AND MEDIAN CORRELATIONS BETWEEN THE FIELD AND RECONSTRUCTED DATA OF THREE TYPES

Data type	Mean correlation	Median correlation
Baseline data	87.9%	89.3%
Missing data in the training subarea	89.8%	91.0%
Missing data in the testing subarea	86.4%	87.9%

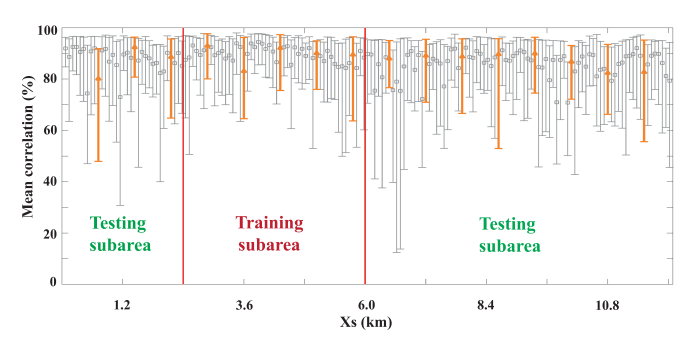


Fig. 5. Correlation between the field data and the constructed data as a function of shot position Xs, for missing data (gray color) and baseline data (orange color). At each shot position, the vertical bar denotes the range of the correlations, and the square or triangle indicates the mean value.

[Fig. 4(c) and (d)] compares the common shot slices (gather), and the bottom pair [Fig. 4(e) and (f)] compares the common receiver slices, respectively. The slices in the left side of the figure are from the sparsely sampled input data cube, with missing traces shown as vertical white stripes in Fig. 4(a) and (e) and no data in Fig. 4(c) since all its traces are missing. The missed field data from Fig. 4(c) are shown in Fig. 3(d). The slices in the right side of Fig. 4 are from the reconstructed data cube. The black wiggle traces in Fig. 4(f) are examples of the reconstructed seismic traces, at the same location as the white stripes in Fig. 4(e).

To evaluate the effectiveness of the SRT2D-ResU-Net quantitatively, we calculate the correlations between the field and reconstructed data for all the missing and baseline traces. As shown in Table I, the average correlation, measured by mean or median, is higher than 85% for the baseline data and missing data from the field marine data set. Interestingly, for this case, the performance of our method for the baseline data is very similar to that for the reconstructed missing data.

Fig. 5 shows the variation in the correlation as a function of shot position, for the missing data (gray color) and baseline data (orange color). Each of the vertical bars in the figure denotes the range of the correlation coefficients of all data traces at the shot position, and each small square (for missing data) or small triangle (for baseline data) indicates the mean value of the correlation coefficients. At all shot positions, the mean correlation is skewed toward the high correlation side, or more high-correlation traces than low-correlation traces everywhere. As expected and statistically, the training subarea has high mean values and narrow ranges of the correlations than that of the testing subarea.

In the testing subarea, as we move farther from the training area, the correlations decrease slightly in trend, and with

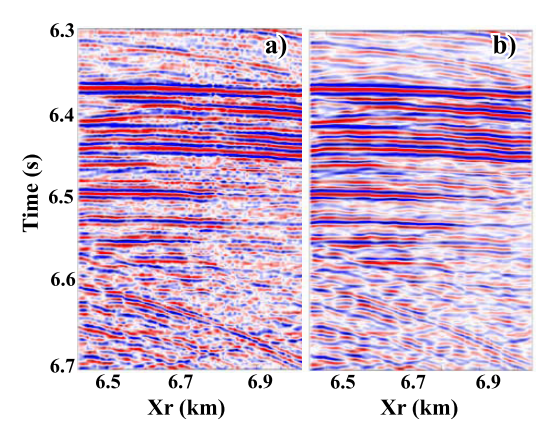


Fig. 6. Comparison between two common shot slices at a baseline location (Xs = 6.48 Km). (a) From the field data cube. (b) From the reconstructed data cube. The field data at all baseline locations are excluded from training the network. The mean correlation between all traces of the two slices is 88%.

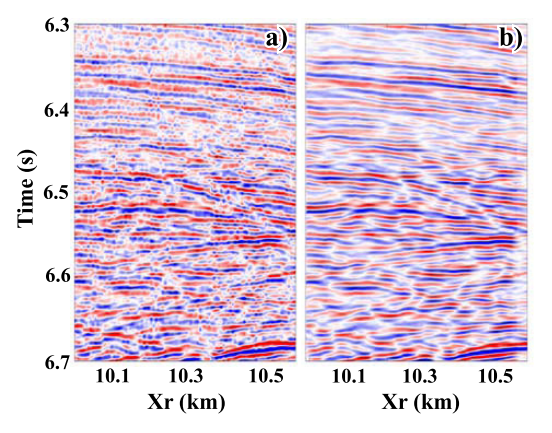


Fig. 7. Comparison between two common shot slices at a "missing data" location (Xs = 10.01 Km). (a) From the field data cube. (b) From the reconstructed data cube. The mean correlation between all traces of the two slices is 70.8%, which is around the bottom level of all missing data slices.

many up and down variations throughout the testing subarea. The slight decrease trend implies that the data features, which the reconstruction relies on, change slowly with the increasing distance from the training subarea. The up and down pattern, likely due to factors such as the data noise level, might have strong local influences on the reconstruction results. In the testing subarea, the correlations based on the baseline data and the missing data show similar distributions, suggesting that the baseline reference gives an effective evaluation on the performance of the trained network.

Fig. 6 shows the comparison of the common shot (gathers) slices of the true field data and reconstructed data, at a baseline location (Xs = 6.48 km). The mean value of the correlation coefficients between all trace pairs at this shot location is 88%, which is slightly higher than the average level of all baseline slices. Clearly, the field data slice has many more short-wavelength or spotty features, in comparison to the reconstructed seismic slice. These short-wavelength features may be very important short-wavelength signals (e.g., due to pinch-outs, fractures, and faults), or noises and artifacts.

Fig. 7 shows another comparison of the common shot slices of the true field data and reconstructed data, at a missing data location (Xs = 10.01 km). The mean correlation of all trace

pairs at this shot location is around 71%, the lowest level of all reconstructed shot slices in this test. The low correlation is likely due to the presence of spotty features over the field data slice shown in Fig. 7(a). Our method is able to reconstruct most of the large events in the field data, even at this shot location of the lowest mean correlation.

#### V. DISCUSSION

Reconstructing missing seismic traces is an interpolation process based on the connectivity of seismic signals among measured data over the survey area. An interpolated seismic trace can never be as trustworthy as the field seismic trace acquired at the same location. Hence, before using a reconstructed seismic data, we must assess its fidelity. Since all missing traces of field data have no true values, we must find a way to establish the reference for assessing the reconstruction of sparsely sampled field data. This has led to our devised baseline reference, which is a widely used tool for quantifying the performance of new methods.

In our study, the baseline reference consists of a small number of observed seismic data traces distributed regularly over the entire survey area. The baseline traces are excluded from the training process and used only for assessing the quality of the reconstructed traces. To give an unbiased assessment about the change in the signal connectivity between the training and testing subareas, the baseline traces should be regularly spaced over the entire survey area. The baseline reference has the potential to be incorporated in other reconstruction tasks.

We use correlation coefficient to evaluate the reconstructed missing traces against the true values, because correlation is among the most widely used measure of similarity in geophysics (e.g., [1], [2]). For the field marine data set, reconstruction of sparsely sampled seismic data using our ML algorithm has resulted in a high level of correlation with the true values, largely due to the high SNR of the marine data set. Users of the reconstructed seismic data should be aware of their limitations. For example, most lateral interpolations tend to smooth data features laterally, thus suppress vertically aligning or spotty features that could be important.

In this study, the relatively small training data set in the "in situ training and prediction" workflow might limit the potential of generalizing the trained network. Nevertheless, the results of our trained models yield a reasonable performance in our tests conducted so far.

### VI. CONCLUSION

We propose a new residual U-Net ML network named SRT2D-ResU-Net, to reconstruct sparsely sampled 2-D seismic data in the SRT domain. Such SRT domain retains a high level of connectivity for subsurface signals in seismic data. Instead of finding a single neural network for reconstructing sparsely sampled seismic data universally, we develop an "in situ training and prediction" workflow by dividing the acquisition area into two nonoverlapping parts. We train the network using regularly sampled data in the training subarea and reconstruct the missing traces in the sparsely sampled testing subarea. To establish a reference base for analyzing the changing data features from the training to the testing subareas, and to evaluate the reconstruction of the missing traces,

we devise a baseline reference which consists of a tiny portion of the field data excluded from the training and reconstruction processes. For a field marine seismic data set, the average correlation between the reconstructed missing traces and the true answers of the baseline reference is over 85%, indicating the effectiveness of our SRT2D-ResU-Net in the training and prediction stages. In this case, the reconstructed traces show similar trends between their correlations with the baseline data and the missing data, indicating that the baseline reference is feasible for evaluating ML networks for field data.

#### ACKNOWLEDGMENT

The authors would like to thank three anonymous Reviewers and Editor-in-Chief Dr. Avik Bhattacharya for their insightful comments. Zhehao Li processed the field data.

### REFERENCES

- R. E. Sheriff and L. P. Geldart, Exploration Seismology. Cambridge, U.K.: Cambridge Univ. Press, 1995.
- [2] H. Zhou, Practical Seismic Data Analysis. Cambridge, U.K.: Cambridge Univ. Press, 2014.
- [3] X. Campman et al., "Sparse seismic wavefield sampling," Lead. Edge, vol. 36, pp. 654–660, Aug. 2017.
- [4] F. J. Herrmann, D. Wang, G. Hennenfent, and P. P. Moghaddam, "Curvelet-based seismic data processing: A multiscale and nonlinear approach," *Geophysics*, vol. 73, no. 1, pp. A1–A5, Jan. 2008.
- [5] N. Gulunay and R. E. Chambers, "Unaliased f—K domain trace interpolation (UFKI)," in *Proc. SEG Tech. Program Expanded Abstr.*, Jan. 1996, pp. 1461–1464.
- [6] F. J. Herrmann and G. Hennenfent, "Non-parametric seismic data recovery with curvelet frames," *Geophys. J. Int.*, vol. 173, no. 1, pp. 233–248, Apr. 2008.
- [7] Y. Jia and J. Ma, "What can machine learning do for seismic data processing? An interpolation application," *Geophysics*, vol. 82, no. 3, pp. V163–V177, May 2017.
- [8] S. Mandelli, F. Borra, V. Lipari, P. Bestagini, A. Sarti, and S. Tubaro, "Seismic data interpolation through convolutional autoencoder," in *Proc. SEG Tech. Program Expanded Abstr.*, Aug. 2018, pp. 4101–4105.
- [9] B. Wang, N. Zhang, W. Lu, and J. Wang, "Deep-learning-based seismic data interpolation: A preliminary result," *Geophysics*, vol. 84, no. 1, pp. V11–V20, Jan. 2019.
- [10] M. A. Nazari Siahsar, S. Gholtashi, V. Abolghasemi, and Y. Chen, "Simultaneous denoising and interpolation of 2D seismic data using data-driven non-negative dictionary learning," *Signal Process.*, vol. 141, pp. 309–321, Dec. 2017.
- [11] S. Yu, J. Ma, X. Zhang, and M. D. Sacchi, "Interpolation and denoising of high-dimensional seismic data by learning a tight frame," *Geophysics*, vol. 80, no. 5, pp. V119–V132, Sep. 2015.
- [12] O. Ronneberger, P. Fischer, and T. Brox, "U-Net: Convolutional networks for biomedical image segmentation," in *Proc. Int. Conf. Med. Image Comput. Comput.-Assist. Intervent*, 2015, pp. 234–241.
- [13] B. Peters, J. Granek, and E. Haber, "Multiresolution neural networks for tracking seismic horizons from few training images," *Interpretation*, vol. 7, no. 3, pp. SE201–SE213, Aug. 2019.
- [14] K. He, X. Zhang, S. Ren, and J. Sun, "Deep residual learning for image recognition," in *Proc. IEEE Conf. Comput. Vis. Pattern Recognit.* (CVPR), Jun. 2016, pp. 770–778.
- [15] Z. Zhang, Q. Liu, and Y. Wang, "Road extraction by deep residual U-Net," *IEEE Geosci. Remote Sens. Lett.*, vol. 15, no. 5, pp. 749–753, May 2018.
- [16] T. Minh Quan, D. G. C. Hildebrand, and W.-K. Jeong, "FusionNet: A deep fully residual convolutional neural network for image segmentation in connectomics," 2016, arXiv:1612.05360. [Online]. Available: http://arxiv.org/abs/1612.05360
- [17] B. Xu, N. Wang, T. Chen, and M. Li, "Empirical evaluation of rectified activations in convolutional network," 2015, arXiv:1505.00853.
  [Online]. Available: http://arxiv.org/abs/1505.00853
- [18] F. Chollet. (2015). Keras. [Online]. Available: https://github.com/fchollet/keras
- [19] M. Abadi et al., "TensorFlow: Large-scale machine learning on heterogeneous distributed systems," 2016, arXiv:1603.04467. [Online]. Available: http://arxiv.org/abs/1603.04467